Kinetics and Catalysis, Vol. 45, No. 4, 2004, pp. 508–518. Translated from Kinetika i Kataliz, Vol. 45, No. 4, 2004, pp. 540–550.

A Quantum Chemical Study of the Molecular Structure of Active Centers and Growth in Ethylene Polymerization in the Catalytic System $LFeCl_2/AlMe_3$ (L = 2,6-Bis-Iminopyridyl)

I. I. Zakharov and V. A. Zakharov

Boreskov Institute of Catalysis, Siberian Division, Russian Academy of Sciences, Novosibirsk, 630090 Russia

Received January 20, 2003

Abstract—Density functional theory with hybrid exchange-correlation functional B3P86 is used to calculate the molecular structures of neutral Fe(II) complexes formed in the $LFeCl_2/AlMe_3$ system (L = tridentate bis(imine)pyridyl ligand). A simplified model of the $LFeCl_2$ complex is used in calculations, where L is replaced by three NH_3 ligands. Parameters of geometric and electronic structures of the complexes $(NH_3)_3FeMe(\mu\text{-}Me)AlMe_3$ (**I**) and $(NH_3)_3FeMe(\mu\text{-}Me)_2AlMe_2$ (**IIA** and **IIB**), which are the structures where the Fe–Me and Fe–μ-Me groups are in one or two perpendicular planes, respectively, were determined. Complexes **II**, which were earlier identified using ^1H NMR spectroscopy, are more stable than complex **I**. Complex **IIB** is strongly polarized (the distances *r*(Fe–μ-Me) and *r*(Al–μ-Me) are 3.70 and 2.08 Å, respectively) and coordinatively unsaturated due to the transfer of the methyl group from $(NH_3)_3FeMe_2$ onto $AlMe_3$. It has significant electron density deficit in the coordination sphere of the transition metal $[(NH_3)_3FeMe]^Q$ (Q = +0.80e). The energetic profile of the reaction of ethylene addition to the Fe–Me bond for the complexes $(NH_3)_3FeMe_2$, **IIA** and **IIB**, was calculated. It was shown that, compared to $(NH_3)_3FeMe_2$, a drastic decrease in the activation energy of ethylene addition is observed in the case of **IIB** (from 135 to 66 kJ/mol). The reason for the more efficient activation of the complexes $LFeMe_2$ by a weak Lewis acid ($AlMe_3$) and for the increased reactivity of the metal-alkyl bond in complex **IIB** compared to the zirconocene complex Cp_2ZrMe_2 is discussed.

INTRODUCTION

Data on the new highly active catalytic systems based on Fe(II) and Co(II) bis(imino)pyridyl complexes for ethylene oligomerization and polymerization has been published recently [1, 2].

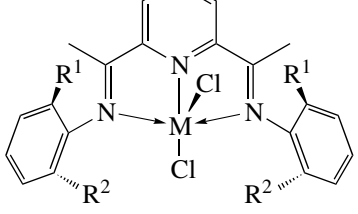

M = Fe, Co
R^1 = Me, *iso*-Pr
R^2 = H, Me, *iso*-Pr

These complexes are activated by methylalumoxane (MAO). It was assumed in [1–3] that in the process of activation of bis(imino)pyryl complexes of Fe(II) and Co(II) by MAO, cationic structures $[LM–CH_3]^+$ (L = bis(imino)pyridyl) are formed as active sites analogously to the activation by metallocene catalysts by MAO and a borate activator.

Intermediates formed in the interaction of $LFeCl_2$ with MAO and $AlMe_3$ were first characterized by NMR in [4–6]. It was also shown that highly active catalysts may be obtained in the activation of $LFeCl_2$ and $LCoCl_2$ by trimethylaluminum and triisobutylaluminum together with MAO. Based on NMR data and data on the high activity of the $LFeCl_2/AlR_3$ catalysts (R = CH_3, *iso*-Bu) in ethylene polymerization, a conclusion has been drawn that the active center in this system is an electroneutral complex rather than cationic intermediate. A precursor of active centers in these systems is the complex $LFeMe(\mu\text{-}Me)_2AlMe_2$ as suggested in [4–6]. It was identified by NMR in those papers.

Theoretical studies of catalysts based on bis(imine)pyridyl complexes of Fe(II) were carried out in [7–9]. However, in these papers the active centers were only considered to be cationic intermediates and the reaction of polymer chain growth with the participation of the cationic active center $(LFeMe)^+$ was calculated. Note that the purely cationic model of the active center leads to strong distortion of the energy profile of the reaction with ethylene in quantum chemical calculations. Recently, researchers came to understand that the active centers of metallocene catalysts should be considered as a whole ionic pair, whose reactivity substantially depends on the nature of the counter-ion [10, 11]. Moreover, as mentioned above, for the catalysts based on $LFeCl_2$ complexes, experimental data were obtained that electroneutral com-

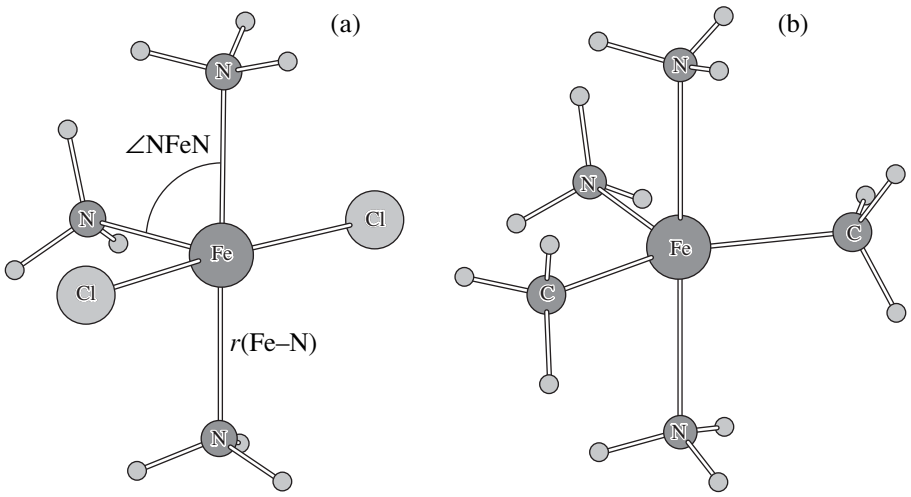

Fig. 1. The calculated model of the $LFeX_2$ complexes (X = Cl, CH_3) in which the tridentate bis(imine)pyridyl ligand is replaced by three ligands of molecular NH_3: (a) model complex $(NH_3)_3FeCl_2$, (b) model complex $(NH_3)_3FeMe_2$.

plexes $LFeMe(\mu\text{-}Me)_2AlMe_2$, which were identified by NMR spectroscopy, can be active center precursors.

Taking these data into account, we carried out density functional theory (DFT) quantum chemical calculation of the structure of a number of electroneutral Fe(II) complexes formed in the $LFeCl_2/AlMe_3$ systems and analyzed the interaction of these complexes with ethylene.

METHOD AND THE CHOICE OF THE INITIAL MODEL

In quantum chemical calculation, we used the DFT method with hybrid exchange-correlation functional B3P86 [12, 13]. Geometry optimization of the structure of the ethylene π-complex, the transition state (TS) in the reaction of ethylene, and the reaction product was carried out using the effective potential (LANL2) for the inner shells of Fe and Zr atoms. In the calculation we used extended double-ξ basis(DZ) for valence *nd*, $(n + 1)s$, and $(n + 1)p$ orbitals of metals and atomic 1*s*, 2*s*, and 2*p* orbitals of H, C, and N [14]. The same variant of calculation in the Gaussian 92 program package [15] is characterized by the abbreviation B3P86/LANL2-DZ. The charges of atoms were calculated using the analysis of Mulliken orbital population. Open shells were calculated using unrestricted SCF (uB3P86/LANL2-DZ).

In the calculation, we used a simplified model of the $LFeX_2$ complexes (X = Cl, CH_3) where the tridentate bis(imine)pyridyl ligand in the real complex is replaced by three molecular NH_3 ligands laying in the same plane (Fig. 1). Valence angles NFeN in such a model complex are 90° and the Fe–N bonds are equivalent. From the electronic standpoint, three unshared electron pairs of NH_3 molecules model unshared electron pairs of the tridentate bis(imine)pyridyl ligand, which substantially simplifies quantum chemical calculations while preserving the correct electronic state of Fe(II) with d^6-electron configuration.

RESULTS AND DISCUSSION

Calculation of the Molecular Structure of $LFeX_2$ Complexes (X = Cl, CH_3)

For the complex $(NH_3)_3FeCl_2$, three electron states are possible (singlet, triplet, and quintet). For the Fe(II) complexes close-laying states with different spin multiplicity are experimentally observed [16]. We calculated all the three spin states of the $(NH_3)_3FeCl_2$ complex. Table 1 shows the results of these calculations. It can be seen that the high-spin state of the $(NH_3)_3FeCl_2$ complex ($S = 2$) is energetically more stable. The calculated value of the spin density [ρ_s(Fe) = 3.74 e] points to the fact that unpaired electrons are localized at the main iron cation. This agrees with experimental data that the real Fe(II) complex with tridentate bis(imine)pyridyl ligands are paramagnetic [5]. The calculated bond lengths *r*(Fe–Cl) and *r*(Fe–N) agree with XRD data [3]. All these facts justify the use of the model complex $(NH_3)_3FeCl_2$ instead of real Fe(II) chloride complex with tridentate bis(imine)pyridyl ligands in quantum chemical calculations (Fig. 1a).

Under conditions of polymerization in the interaction of the bis(imine)pyridyl chloride complex of Fe(II) with $AlMe_3$, the alkylation reaction with the formation of the Fe(II) methyl derivatives occurs [4–6]. Therefore, we carried out quantum chemical calculations of the $(NH_3)_3FeMe_2$ complex (Fig. 1b) in various spin states ($S = 0, 1, 2$). The results of calculations are sum-

Table 1. Parameters of the geometric and electron structures of the complexes $(NH_3)_3FeCl_2$ and $(NH_3)_3FeMe_2$ (Fig. 1) in various spins states (S = 0, 1, 2) calculated by the DFT/LANL2-DZ method

Geometric and electron parameters of the complex	$S = 0$		$S = 1$		$S = 2$	
	$(NH)_3FeCl_2$	$(NH_3)_3FeMe_2$	$(NH)_3FeCl_2$	$(NH_3)_3FeMe_2$	$(NH)_3FeCl_2$	$(NH_3)_3FeMe_2$
r, Å*						
Fe–Cl	2.33	–	2.33	–	2.40	–
Fe–CH_3	–	1.99	–	2.08	–	2.12
Fe–N	2.00	2.09	2.09	2.14	2.19	2.34
N–H	1.02	1.02	1.02	1.02	1.02	1.02
Spin density at Fe, ρ_s(e)	0.0	0.0	2.05	2.12	3.74	3.84
q(Fe)	+0.10	+0.20	+0.22	+0.52	+0.41	+0.64
q(Cl)	–0.44	–	–0.43	–	–0.48	–
$q(CH_3)$	–	–0.32	–	–0.49	–	–0.52
$q(NH_3)$	+0.26	+0.15	+0.21	+0.15	+0.18	+0.13
ε_i(HOMO), eV**	–5.7	–4.7	–	–	–	–
Dipole momentum, μ, D	4.06	8.11	3.95	3.20	4.98	4.85
Full energy, at. units	–394.38980	–374.09201	–394.39691	–374.12402	–394.42617	–374.15038

* Experimental values of the bond lengths r(Fe–Cl) = 2.30 Å and r(Fe–N) = 2.11–2.27 Å in bis(imine)pyridyl chloride complex of Fe(II) [3].
** For the complex Cp_2ZrMe_2, the calculated value of ε_i(HOMO) = –7.1 eV.

marized in Table 1. Note that, for the methyl complex $(NH_3)_3FeMe_2$, the high-spin state (S = 2) is the most energetically stable as for the chloride complex $(NH_3)_3FeCl_2$.

DFT Calculation of the Energy Profile of the Reaction of Ethylene Addition for the Complexes $(NH_3)_3FeMe_2$ and Cp_2ZrMe_2

As shown in [17], the electronic mechanism of the reaction of ethylene insertion into a metal–alkyl bond is determined by the transfer of electron density from bonding σ orbitals of the metal–alkyl (M–R) bond onto the antibonding π* orbital of ethylene coordinated to the metal ion. The nature of the insertion reaction depends on the nature of the catalyst through the lability (or the strength) of the M–R bond. The reactivity index in the ethylene insertion into a metal–alkyl bond can be the energy position of the highest occupied molecular orbital (HOMO), the contribution to which is greatest from the M–R bond. Table 1 shows the calculated value of ε_i(HOMO) = –4.7 eV for the $(NH_3)_3FeMe_2$ complex. Note that the calculated value of ε_i(HOMO) for the zirconocene complex Cp_2ZrMe_2 is –7.1 eV. This value is much lower than ε_i(HOMO) calculated for the complex $(NH_3)_3FeMe_2$. Comparison of the ε_i(HOMO) values for the $(NH_3)_3FeMe_2$ and Cp_2ZrMe_2 complexes and allows us to suggest that the Fe–CH_3 bond has the highest reactivity in ethylene addition compared to the Zr–CH_3 bond.

To support the conclusion that the potential reactivity of the $(NH_3)_3FeMe_2$ complex is higher than that of the Cp_2ZrMe_2 complex in ethylene addition, we carried out DFT calculations of energy profiles for ethylene

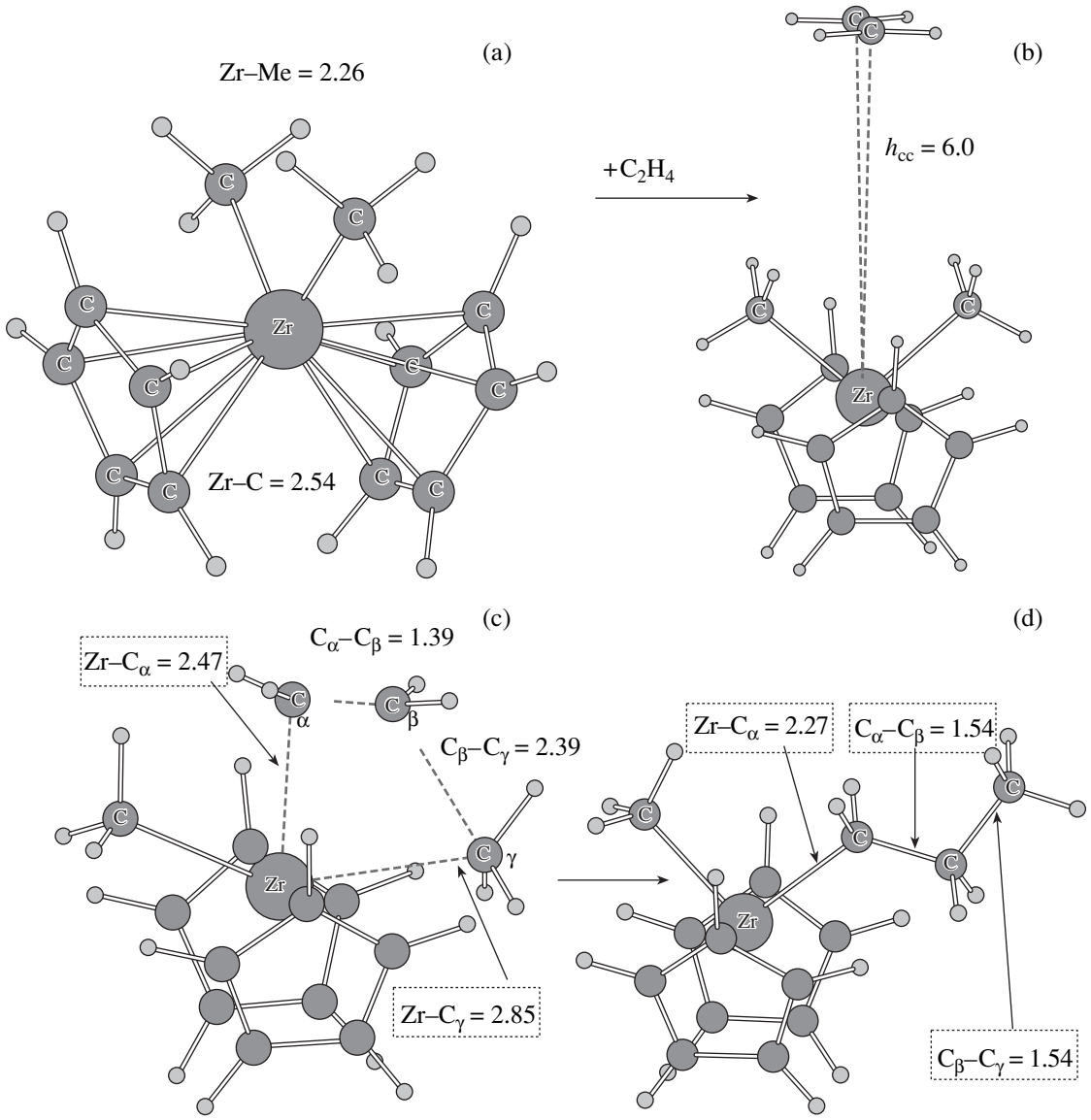

Fig. 2. Quantum chemical calculation (DFT/LANL2-DZ) of molecular structures of (a) the Cp_2ZrMe_2 complex, (b) π-complex with ethylene, (c) TS of ethylene *cis*-insertion, (d) insertion product with *trans* configuration, formed at stages b ⟶ c ⟶ d in the interaction of ethylene with the Cp_2ZrMe_2 complex (a). The calculated interatomic distances are given in angstroms (see Table 2).

interaction with $(NH_3)_3FeMe_2$ and Cp_2ZrMe_2 complexes along the reaction coordinate:

Active center + ethylene ⇒ π-complex ⇒ transition state ⇒ product of insertion.

Calculation of the energy profile of this reaction can be reduced to the calculation of four stationary points on the energy surface:

(a) The activation energy of the active center and ethylene;

(b) The energy of the π-complex with ethylene;

(c) The energy of the transition state (TS) of ethylene *cis*-insertion; and

(d) The energy of the insertion product.

Figures 2 and 3 show the results of B3P86/LANL2-DZ calculation of the molecular structures of these stationary points for the reaction of ethylene interaction with the Cp_2ZrMe_2 complex (the ground $^1A_1$ singlet state, $S = 0$) (Fig. 2) and with the $(NH_3)_3FeMe_2$ complex (the ground $^5A'$ quintet state, $S = 2$) (Fig. 3). The energy profile of the reaction of ethylene addition is shown in Fig. 4 and the results of calculations are summarized in Table 2. When analyzing the results of calculation of the reaction of ethylene addition to the M–CH_3 bond, we should note for the complexes Cp_2ZrMe_2 and $(NH_3)_3FeMe_2$ that the $(NH_3)_3FeMe_2$ complex may

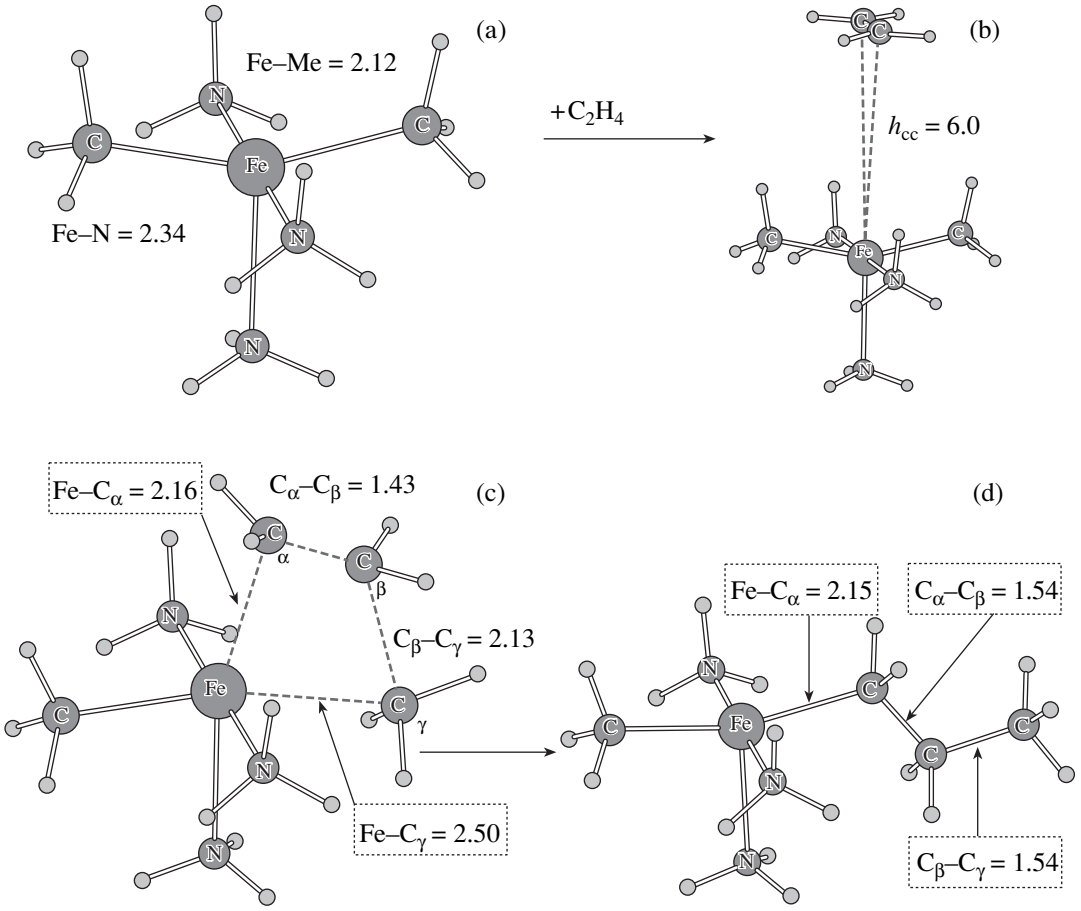

Fig. 3. Quantum chemical calculation (DFT/LANL2-DZ) of molecular structures of (a) the $(NH_3)_3FeMe_2$ complex, (b) π-complex with ethylene, (c) TS of ethylene *cis*-insertion, (d) insertion product with *trans* configuration formed at stages b ⟶ c ⟶ d in the interaction of ethylene with the $(NH_3)_3FeMe_2$ complex (a). Optimization of molecular structures corresponds to the high-spin state of the Fe(II) ion (S = 2). The calculated interatomic distances are shown in angstroms (see Table 2).

potentially be a more efficient catalyst for ethylene polymerization compared to Cp_2ZrMe_2. This is evident from the following results:

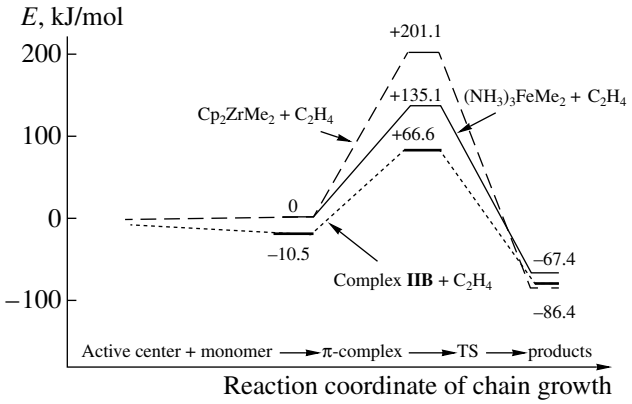

Fig. 4. Calculated (DFT/LANL2-DZ) profiles of the potential energy for the reactions of interaction with ethylene for the complexes Cp_2ZrMe_2 and $(NH_3)_3FeMe_2$, and for the active center $(NH_3)_3FeMe(\mu\text{-}Me)_2AlMe_2$ (**IIB**).

(1) The calculated energy profile of the ethylene addition reaction (Fig. 4) is characterized by the much lower activation energy of ethylene insertion into the Fe–Me bond (E_p = +135 kJ/mol) than that of the bond Zr–Me (E_p = +201 kJ/mol). Note that for none of the complexes is there a step of ethylene coordination on the energy profile of the reaction (ΔH_π = 0.0 kJ/mol) and therefore the activation energies of the forward reaction of ethylene addition are very high. To decrease the activation energy of ethylene insertion, it is necessary to form the coordinatively unsaturated active center, which is capable of coordinating (activating) ethylene before the insertion step. Such centers may be formed by transfer of the methyl group from the dimethyl complex onto the co-catalyst (e.g., MAO) as it happens in the case of zirconocene systems.

(2) The calculated electron characteristics of the Zr–Me bond in the complex Cp_2ZrMe_2 (ε_i(HOMO) = –7.1 eV, q(Me) = –0.36e) and the Fe–Me bond in the complex $(NH_3)_3FeMe_2$ (ε_i(HOMO) = –4.7 eV, q(Me) = –0.52e) (Table 2) point to the higher lability of the Fe–

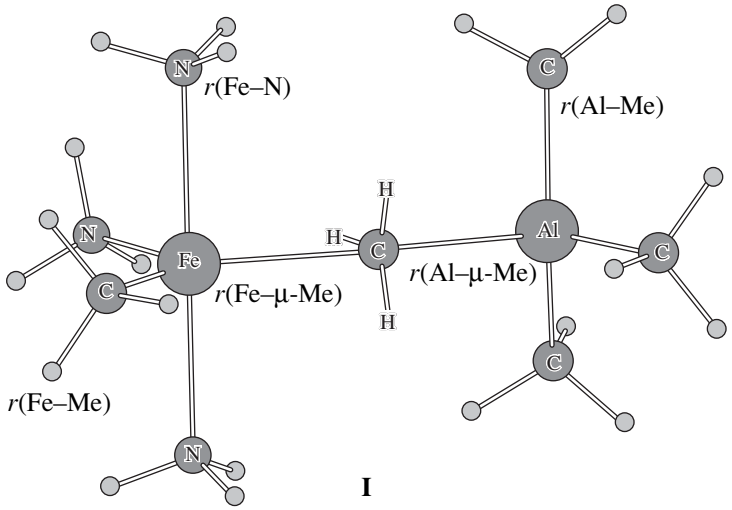

Fig. 5. Molecular structure of the complex $(NH_3)_3(Me)Fe–\mu\text{-}Me–AlMe_3$ (**I**).

Me bond and the possibility of a stronger acid–base interaction of the methyl group (q(Me) = –0.52e) of the $(NH_3)_3FeMe_2$ complex with the Lewis acid center of the cocatalyst.

This comparison of calculated electron characteristics of the metal–alkyl bond in dimethyl complexes of iron and zirconium shows that the reason for such a difference is in the nature of the ligands: valence Cp ligands in the Cp_2ZrMe_2 complex lead to a decrease in the electron density on the central metal atom and an increase in the oxidation state of zirconium from Zr(II) to Zr(IV), whereas electron-donor NH_3 ligands in the dimethyl complex $(NH_3)_3FeMe_2$ do not change the oxidation state of Fe(II). Electron-donor ligands lead to an increase in the electron density on the central atom of the metal, which becomes more capable of providing its electrons for the formation of a metal–alkyl bond. An increased electron density on the central ion Fe(II) leads to the formation of more labile Fe–Me bonds and excessive electron density on the methyl ligands. All of this should result in more facile activation of the $(NH_3)_3FeMe_2$ catalyst compared to the Cp_2ZrMe_2 catalyst and makes it possible to explain recent experimental data on the possibility of activation of the bis(imine)pyridyl $LFeCl_2$-complex by a weak Lewis acid, trialkylaluminum [4–6].

Correspondingly, the introduction of electron-donor substituents in the cyclopentadienyl ligand of zirconocene complexes may also lead to the more efficient activation of these complexes. This fact was experimentally found in [18], where ethylene polymerization was studied on the $(CpR)_2ZrCl_2$ catalyst with various electron-donor substituents R = Me, Et, *iso*-Pr, *tert*-Bu, $SiMe_3$, and CMe_2Ph. Ethylalumoxane was used as an activator/cocatalyst. These studies showed that the activity of the catalytic system increases with an increase in the electron-donor ability of R substituents [18].

Molecular Structure of Complexes Formed in the Reaction of $(NH_3)_3FeMe_2$ with Trimethylaluminum

According to ^1H and ^2H NMR spectroscopic data, in the interaction of $LFeCl_2$ with $AlMe_3$, molecular electroneutral complexes $LFeMe(\mu\text{-}Me)_2AlMe_2$ are formed [4–6]. We used the B3P86/LANL2-DZ method to calculate the parameters of the geometric and electron structure of donor-acceptor complexes $(NH_3)_3FeMe(\mu\text{-}Me)AlMe_3$ (**I**) and $(NH_3)_3FeMe(\mu\text{-}Me)_2AlMe_2$ (**II**) formed as a result of $AlMe_3$ interaction with the $(NH_3)_3FeMe_2$ complex in the spin state S = 2 (Table 3, Figs. 5, 6). The results of calculation show that the formation of complexes **II** occurs with a higher enthalpy, and structures **IIA** and **IIB** with two bridging μ-Me groups (Fig. 6) are more stable than structure **I** with one bridging μ-Me group. According to NMR data, such complexes $LFeMe(\mu\text{-}Me)_2AlMe_2$ (**II**) (L = bis(imine)pyridyl) are formed in the interaction of $LFeCl_2$ with trimethylaluminum [4–6].

The calculated values of equilibrium distances in complex **IIA** (r(Fe–μ-Me) = 2.57 Å and r(Al–μ-Me) = 2.10 Å) point to the fact that in these cases methyl group transfers from $(NH_3)_3FeMe_2$ to $AlMe_3$ with the formation of the polarized complex with two bridging methyl groups $(NH_3)_3FeMe(\mu\text{-}Me)_2AlMe_2$. This polarization reveals itself to a greater extent for complex **IIB** (Fig. 6, Table 3) where the methyl group Fe–Me and the

Table 2. Quantum chemical data of ethylene addition to the Zr–Me bond in the Cp_2ZrMe_2 complex and to the Fe–Me bond in the complex $(NH_3)_3Fe(Me)_2$

Molecular system	DFT/LANL2-DZ calculation of the growth reaction		
	geometric characteristics, Å	electron characteristics	energy characteristics
C_2H_4	r(C=C) = 1.34	μ = 0.0 D	E_{total} = –78.86571 at. units
+			
Cp_2ZrMe_2	r(Zr–Me) = 2.26	ε_i(HOMO) = –7.1 eV	E_{total} = –515.33290 at. units
(Fig. 2a)	r(Zr–C) = 2.57	q(Zr) = +0.96	
⇓		q(Me) = –0.36	
		q(Cp) = –0.12	
π-Complex	h_{cc} = 6.0	$\Delta\rho(C_2H_4)$ = 0.0	E_{total} = –594.19861 at. units
(Fig. 2b)	r(C=C) = 1.34		ΔH_π = 0.0 kJ/mol
⇓			
TS	r(Zr–C_α) = 2.47	q(Zr) = +0.89	E_{total} = –594.12202 at. units
(Fig. 2c)	r(C_α–C_β) = 1.39	q(Cp) = –0.12	E_p = +201.1 kJ/mol
	r(Zr–C_γ) = 2.85	q(C_γ) = –0.23	
⇓			
Insertion product	r(Zr–C_α) = 2.27	q(Zr) = +0.94	E_{total} = –594.23150 at. units
(Fig. 2d)	r(C_α–C_β) = 1.54	q(Cp) = –0.13	ΔH_p = –86.4 kJ/mol
	r(C_β–C_γ) = 1.54	q(Me) = –0.39	
C_2H_4	r(C=C) = 1.34	μ = 0.0 D	E_{total} = –78.86571 at. units
+			
$(NH_3)_3FeMe_2$	r(Fe–Me) = 2.12	ε_i(HOMO) = –4.7 eV	E_{total} = –374.15038 at. units
(Fig. 3a)	r(Fe–N) = 2.34	ρ_s(Fe) = 3.84 e	
		q(Fe) = +0.64	
⇓		q(Me) = –0.52	
		q(NH_3) = +0.13	
		Q[$(NH_3)_3$FeMe] = +0.52	
π-Complex	h_{cc} = 6.0	$\Delta\rho(C_2H_4)$ = 0.0	E_{total} = –453.01609 at. units
(Fig. 3b)	r(C=C) = 1.34		ΔH_π = 0.0 kJ/mol
⇓			
TS	r(Fe–C_α) = 2.16	ρ_s(Fe) = 3.73 e	E_{total} = –452.96462 at. units
(Fig. 3c)	r(C_α–C_β) = 1.43	q(Fe) = +0.55	E_p = +135.1 kJ/mol
	r(Fe–C_γ) = 2.50	q(NH_3) = +0.13	
		q(C_γ) = –0.32	
⇓			
Insertion product	r(Fe–C_α) = 2.15	ρ_s(Fe) = 3.70 e	E_{total} = –453.04176 at. units
(Fig. 3d)	r(C_α–C_β) = 1.54	q(Fe) = +0.61	ΔH_p = –67.4 kJ/mol
	r(C_β–C_γ) = 1.54	q(NH_3) = +0.13	
		q(Me) = –0.52	
		Q($(NH_3)_3$FeMe) = +0.52	

Table 3. Parameters of geometric and electron structures of complexes $(NH_3)_3FeMe(\mu\text{-}Me)AlMe_3$ (**I**) (Fig. 5) and $(NH_3)_3FeMe(\mu\text{-}Me)_2AlMe_2$ (**IIA**) and (**IIB**) (Fig. 6) calculated by the B3P86/LANL2-DZ method

Geometric and electron parameters of the complex ($S = 2$)	Structure of complexes		
	type **I** (Fig. 5)	type **IIA** (Fig. 6)	type **IIB** (Fig. 6)
r, Å			
Fe–Me	2.10	2.13	2.08
Fe–μ-Me	2.32	2.57	3.70
Al–μ-Me	2.18	2.10	2.08
Al–Me	2.03	2.02	2.02
Fe–N	2.28	2.25	2.21
Spin density on Fe, ρ_s(Fe)	3.81	3.80	3.74
q(Fe)	+0.60	+0.40	+0.73
q(Me)	−0.42	−0.44	−0.35
q(μ-Me)	−0.46	−0.46	−0.58
$q(NH_3)$	+0.15	+0.16	+0.14
$Q((NH_3)_3FeMe)$	+0.63	+0.44	+0.80
Dipole momentum μ, D	12.3	8.3	11.7
Full energy, at. units	−496.46130	−496.47601	−496.46664
$(NH_3)_3FeMe_2 + AlMe_3^*$			
ΔH, kJ/mol	–27.4	−66.0	−41.4

* Energy of $AlMe_3$ (r_{Al-C} = 1.98 Å), E_{tot} = –122.30050 at. units calculated by the B3P86/LANL2-DZ method.

μ-methyl groups Fe–$(\mu\text{-}Me)_2$ are in the perpendicular planes. In complex **IIB**, the distance r(Fe–μ-Me) is 3.70 Å, and r(Al–μ-Me) = 2.08 Å. This complex is coordinatively unsaturated (ΔH_π = −12.5 kJ/mol) because of the deficiency of electron density (Q = +0.80e) on the molecular fragment $[(NH_3)_3FeMe]^Q$, which contains the transition metal ion. At the same time for complex **IIA**, the calculated value Q is as low as +0.44e, and the complex is not coordinatively unsaturated (ΔH_π = 0.0 kJ/mol).

Note that the energetic stabilities of both molecular structures **IIA** and **IIB** are about the same (the calculated values of E_{tot} are –496.47601 and –496.46664 at. units, respectively), but their reactivities in ethylene addition are much different.

*Calculation of the Energy Profile of the Reaction of Ethylene Addition to the Fe–CH_3 Bond in the Complexes $(NH_3)_3FeMe(\mu\text{-}Me)_2AlMe_2$ (**IIA** and **IIB**)*

We used the B3P86/LANL2-DZ method to calculate the reaction of ethylene addition to the Fe–CH_3 bond for complexes **IIA** and **IIB** with a general composition $(NH_3)_3FeMe(\mu\text{-}Me)_2AlMe_2$. The results of calculation showed that complex **IIA**, by analogy with the complex $(NH_3)_3FeMe_2$, cannot coordinate ethylene

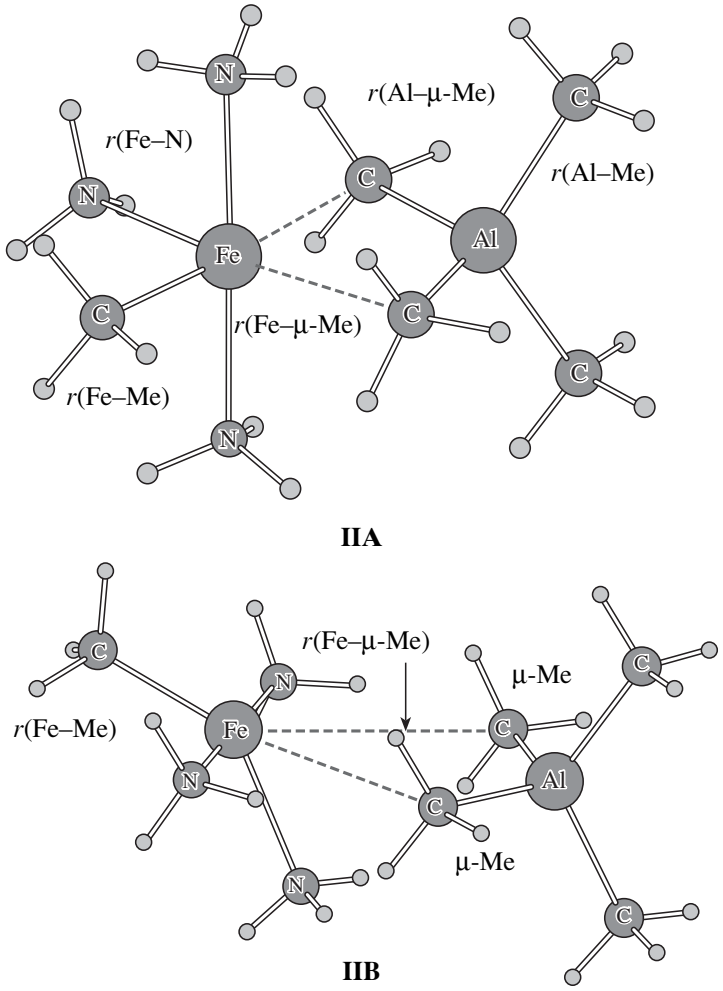

Fig. 6. Molecular structure of complexes **IIA** and **IIB** with the composition $(NH_3)_3Fe_2Me(\mu\text{-}Me)_2AlMe_2$. Fe–Me and Fe–μ-Me groups are in one plane (**IIA**) or in the perpendicular planes (**IIB**).

and, correspondingly, the activation energy of ethylene addition to the Fe–CH_3 bond in this complex is as high as in the initial complex $(NH_3)_3F_2Me_2$. At the same time complex **IIB**, which has the same composition as **IIA** but different geometric and electron structures, can coordinate ethylene with its further insertion into the Fe–Me bond with a lower activation energy. Figure 7 and Table 4 show the results of calculation of various stages of the reaction of ethylene addition to the Fe–Me bond for complex **IIB**. The calculated activation energy of ethylene addition (E_p) to the Fe–Me bond is +66.6 kJ/mol (Fig. 4), which is much lower than for the nonactivated complex $(NH_3)_3FeMe_2$ (E_p = +135.1 kJ/mol). This is primarily due to the formation of a coordination vacancy on the active center, which is necessary for the interaction with ethylene. Indeed, the results of calculations (Table 4, Figs. 4, 7) show that in the interaction of ethylene with complex **IIB**, the π-complex is formed at the first stage with a heat of ΔH_π = –10.5 kJ/mol. The coordination vacancy is formed due to the transfer of the methyl group from $(NH_3)_3FeMe_2$ onto $AlMe_3$. As a result, a strongly polarized molecular system is formed with the deficiency of electron density on the molecular part which contains the transition metal ion (Fe), and with excess electron density on the molecular part which contains the ion of the nontransition metal (Al). The deficiency of electron density in the coordination sphere of the transition metal increases from +0.44 to +0.80e when one passes from complex **IIA** to **IIB** (Table 3). It is reasonable that the ethylene molecule characterized as a π-electron base would more efficiently enter the coordination sphere of a transition metal, which has the higher deficiency of electron density, leading to the formation of the π-complex and to a decrease in the activation energy of ethylene addition to the Fe–Me bond in complex **IIB**.

Thus, in the catalytic system $LFeCl_2/AlMe_3$, complexes like **IIB** with deficient electron density in the coordination sphere of the transition metal can be considered as one of the types of electroneutral molecular

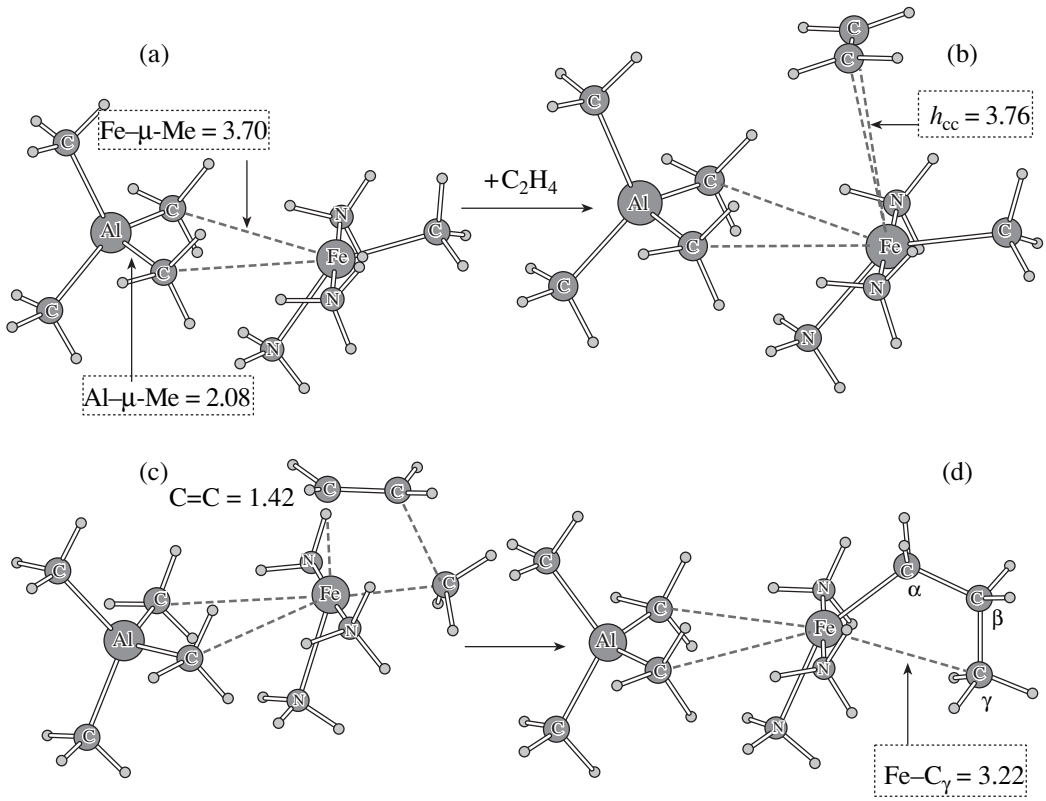

Fig. 7. Quantum chemical calculation (DFT/LANL2-DZ) of the stages (b ⟶ c ⟶ d) on the active complex **IIB** (a). Optimization of molecular structures of (a) the active complex **IIB**, (b) π-complex with ethylene, (c) TS of *cis*-insertion of ethylene, (d) the product of ethylene *cis*-insertion corresponding to the high-spin state of the iron ($S = 2$). The calculated interatomic distances are shown in Å (see Table 4).

Table 4. Quantum chemical data for ethylene addition to the Fe–Me bond in complex **IIB** with the composition $(NH_3)_3FeMe(\mu\text{-}Me)_2AlMe_2$

Molecular system	B3P86/LANL2-DZ calculation		
	geometric characteristics, Å	electron characteristics	energy characteristics
C_2H_4	r(C=C) = 1.34	μ = 0.0 D	E_{tot} = –78.86571 at. units
+			
Complex **IIB**	r(Fe–Me) = 2.08	ρ_s(Fe) = 3.74 e	E_{tot} = –496.46664 at. units
(Fig. 7a)	r(Fe–N) = 2.21	q(Fe) = +0.73	
	r(Fe–μ-Me) = 3.70	q(Me) = –0.35	
	r(Al–μ-Me) = 2.08	$q(NH_3)$ = +0.14	
	r(Al–Me) = 2.02	q(μ-Me) = –0.58	
		$Q((NH_3)_3FeMe)$ = +0.80	
		μ = 11.7 D	
⇓			
π-Complex (Fig. 7b)	h_{cc} = 3.76	$\Delta\rho(C_2H_4)$ = +0.03	E_{tot} = –575.33634 at. units
	r(C=C) = 1.34		ΔH_π = –10.5 kJ/mol
⇓			
TS	r(Fe–C_α) = 2.21	ρ_s(Fe) = 3.66 e	E_{tot} = –575.30700 at. units
(Fig. 7c)	r(C_α–C_β) = 1.42	q(Fe) = +0.54	E_p = +66.6 kJ/mol
	r(Fe–C_γ) = 2.31	$q(NH_3)$ = +0.15	
⇓			
Insertion product	r(Fe–C_α) = 2.11	ρ_s(Fe) = 3.74 e	E_{tot} = –575.36488 at. units
(Fig. 7d)	r(C_α–C_β) = 1.56	q(Fe) = +0.64	ΔH_p = –85.4 kJ/mol
	r(C_β–C_γ) = 1.54	$q(NH_3)$ = +0.15	
	r(Fe–C_γ) = 3.22	$q(C_3H_7)$ = –0.29	
	r(Fe–μ-Me) = 3.74	$Q((NH_3)_3FeR)$ = +0.80	
	r(Al–μ-Me) = 2.08	R ≡ C_3H_7	
	r(Al–Me) = 2.02	μ = 12.2 D	

structures which are the active centers of polymerization. Note also that the calculated value of the activation energy of ethylene addition to complex **IIB** (E_p = +66 kJ/mol) is still rather high compared to usual experimental values for the activation energy of chain growth. Our preliminary analysis shows that in these systems the formation of more active centers due to the interaction of $LFeCl_2$ with several $AlMe_3$ molecules is possible. The results of these calculations will be reported in the next paper.

ACKNOWLEDGMENTS

This work was supported by INTAS (grant no. 00-00841).

REFERENCES

1. Small, B.L., Brookhart, M., and Bennett, A.M.A., *J. Am. Chem. Soc.*, 1998, vol. 120, p. 4049.
2. Britovsek, G.J.P., Gibson, V.C., Kimberley, B.S., Maddox, P.J., McTavish, S.J., Solan, G.A., White, A.J.P., and Williams, D.J., *Chem. Commun*, 1998, no. 7, p. 849.
3. Britovsek, G.J.P., Bruce, M., Gibson, V.C., Kimberley, B.S., Maddox, P.J., Mastroianni, S., McTavish, S.J., Redshaw, C., Solan, G.A., Stroemberg, S., White, A.J.P., and Williams, D.J.J., *J. Am. Chem. Soc.*, 1999, vol. 121, p. 8728.
4. Talzi, E.P., Babushkin, D.E., Semikolenova, N.V., Zudin, V.N., and Zakharov, V.A., *Kinet. Katal.*, 2001, vol. 42, no. 2, p. 165.
5. Talsi, E.P., Babushkin, D.E., Semikolenova, N.V., Zudin, V.N., Panchenko, V.N., and Zakharov, V.A., *Macromol. Chem. Phys.*, 2001, vol. 202, p. 2046.
6. Semikolenova, N.V., Zakharov, V.A., Talsi, E.P., Babushkin, D.E., Sobolev, A.P., Echevskay, L.G., and Khysniyarov, M.M., *J. Mol. Catal., A: Chem.*, 2002, vols. 182–183, p. 283.
7. Deng, L., Margl, P., and Ziegler, T., *J. Am. Chem. Soc.*, 1999, vol. 121, p. 6479.
8. Griffiths, E.A.H., Britovsek, G.J.P., Gibson, V.C., and Gould, I.R., *Chem. Commun*, 1999, no. 14, p. 1333.
9. Khoroshun, D.V., Musaev, D.G., Vreven, T., and Morokuma, K., *Organometallics*, 2001, vol. 20, p. 2007.
10. Schaper, F., Geyer, A., and Brintzinger, H.H., *Organometallics*, 2002, vol. 21, p. 473.
11. Nifant'ev, I.E., Ustynyuk, L.Yu., and Laikov, D.N., *Organometallics*, 2001, vol. 20, p. 5375.
12. Perdew, J.P., *Phys. Rev. B: Condens. Matter*, 1986, vol. 33, p. 8822.
13. Becke, A.D., *J. Chem. Phys.*, 1993, vol. 98, p. 1372.
14. Hay, P.J. and Wadt, W.R., *J. Chem. Phys.*, 1985, vol. 82, p. 270.
15. Frisch, M.J., Trucks, M.A., Schlegel, H.B., Gill, P.M.W., Johnson, B.G., Wong, M.W., Foresman, J.B., Robb, M.A., Head-Gordon, M., Replogle, E.S., Gomperts, R., Andres, J.L., Raghavachari, K., Binkley, J.S., Gonzalez, C., Martin, R.L., Fox, D.J., Defrees, D.J., Baker, J., Stewart, J.J.P., and Pople, J.A., *Gaussian 92*, DFT, Revision G.2, Pittsburgh, PA: Gaussian, 1993.
16. Hauser, A., Jeftic, J., Romstedt, H., Hinek, R., and Spiering, H., *Coord. Chem. Rev.*, 1999, vols. 190–192, p. 471.
17. Zakharov, I.I., Zakharov, V.A., and Zhidomirov, G.M., *Kinet. Katal.*, 1994, vol. 35, no. 1, p. 74.
18. Mohring, P.C. and Coville, N.J., *J. Mol. Catal.*, 1992, vol. 77, p. 41.